Exp. Theo. NANOTECHNOLOGY 10 (2026) 81-91 https://doi.org/10.56053/10.1.81

Correlation between microstructure and optical transparency of PLD-derived nanostructured La_2O_3

Hussian Fakhry[1], *Mohammed RASHEED*[2,*], *Odai N. Salman*[1], *Raid A. Ismail*[1]

[1]Applied Sciences Department, University of Technology- Iraq, Baghdad 10066, Iraq
[2]Production Engineering & Metallurgy College, University of Technology- Iraq, Baghdad, Iraq
[*]) Email: rasheed.mohammed40@yahoo.com

Received 2/10/2025, *Received in revised form* 22/11/2025, *Accepted* 29/12/2025, *Published* 15/1/2026

Lanthanum oxide (La_2O_3) thin films were synthesized using the pulsed laser deposition (PLD) method to explore their potential in optoelectronic device applications. High-purity La_2O_3 pellets were fabricated by palletisation with polyvinyl alcohol (PVA) as a binder and subsequently sintered to enhance mechanical strength. The deposition is carried out using a Nd:YAG laser (λ = 532 nm, 1000 mJ, 6 Hz) onto fluorine-doped tin oxide (FTO) substrates under a vacuum pressure of 10^{-2} torr. Post-growth analyses included X-ray diffraction (XRD) to determine the crystalline structure, atomic force microscopy (AFM) for surface topography, Fourier-transform infrared spectroscopy (FTIR) and the vibrational characteristics of the La_2O_3 films were examined using Raman spectroscopy, and their optical response, including absorption and transmittance behaviour, is evaluated through UV–Vis spectroscopic analysis. Results confirmed the formation of polycrystalline films with homogeneous grain distribution and minimal surface roughness. Optical absorption studies demonstrated high transparency in the visible spectrum and revealed a direct band gap energy of 3.80 eV highlighting the suitability of La_2O_3 thin films for optoelectronic and photonic applications.

Keywords: La_2O_3 NPs; FESEM; XRD.

1. INTRODUCTION

Nanotechnology has become a cornerstone of modern materials science, enabling the design and control of matter at the nanoscale to achieve novel physical, chemical, and functional properties [1-3] Nanostructured materials, in particular, exhibit size-dependent optical, electrical, and thermal behaviours that differ significantly from their bulk counterparts, making them highly attractive for next-generation electronic, photonic, and energy-related applications [4, 5]. Within this context, rare-earth oxides such as lanthanum oxide (La_2O_3) have gained increasing attention due to their

multifunctional properties [6-8]. Lanthanum oxide (La_2O_3), a rare-earth sesquioxide, has attracted significant research interest owing to its unique combination of physical and chemical properties, including a high dielectric constant (~27), wide optical band gap (>5 eV), excellent chemical inertness, and thermal stability [9-11]. These features render La_2O_3 a promising candidate for diverse technological applications such as gate dielectrics in complementary metal–oxide–semiconductor (CMOS) devices [12], protective coatings for optical components [13], and active layers in ultraviolet (UV) photodetectors [14]. Furthermore, its inherently low phonon energy minimizes non-radiative recombination, thereby enhancing the efficiency of optoelectronic devices [15]. Despite these advances, the literature still lacks comprehensive investigations that systematically combine microstructural, morphological, vibrational, optical, and thermal analyses of La_2O_3 films deposited via PLD [16]. Many existing studies focus only on structural or optical aspects, leaving a gap in the holistic understanding of how deposition parameters govern multifunctional properties [17,18]. Moreover, limited attention has been given to thermal behaviour, such as diffusivity and conductivity, which is vital for applications involving heat dissipation and stability in electronic and photonic devices [19,20]. The main objective is to establish a clear correlation between deposition parameters and film performance, providing valuable insights for optimizing La_2O_3 NPs thin films for next-generation optoelectronic, dielectric, and photonic devices. By integrating structural, optical, vibrational, and thermal analyses, this research delivers a comprehensive dataset that not only benchmarks La_2O_3 against related rare-earth oxide films but also offers practical guidance for their future technological deployment. This study fabricates La_2O_3 nanoparticles thin films via PLD under controlled conditions and employs XRD, AFM, FTIR, Raman, and UV–vis spectroscopy for comprehensive characterization.

2. MATERIALS AND METHODS

Polyvinyl alcohol (PVA) is employed as a binder to improve the mechanical integrity of the pressed La_2O_3 pellets. For this purpose, 1 g of PVA powder is dissolved in 10 mL of distilled water under constant magnetic stirring at 65 °C. The mixture is stirred and heated for about 30 minutes to achieve complete dissolution, yielding a uniform 10 wt.% PVA binder solution. To fabricate the La_2O_3 pellet target, 0.2 mL of the prepared PVA binder is thoroughly mixed with 2 g of high-purity La_2O_3 powder using an agate mortar and pestle to ensure homogeneity. The blended mixture is loaded into a stainless-steel mold and subjected to uniaxial pressing at 1 MPa (10 tons) for 5 minutes with a hydraulic press, producing a compact green pellet of ~0.8 cm diameter and 0.6 cm thickness. The pellet is subsequently sintered in an electric furnace at 400 °C for 2.5 hours under controlled heating, improving particle bonding and ensuring sufficient mechanical strength for pulsed laser ablation. La_2O_3 NPs thin films are deposited using a pulsed laser deposition (PLD) system with an Nd:YAG laser (λ = 532 nm, pulse energy 1000 mJ, 6 Hz). The beam, focused by a 6 mm lens, delivered a fluence of 12.50 J/cm² onto the pellet target at a 45° incidence inside a stainless-steel vacuum chamber maintained at 10^{-2} torr and 14 °C. A plasma plume formed during ablation transported species to the substrate placed 2.5 cm from the target. Each deposition involved 1000 pulses. La_2O_3 targets are separately ablated under identical conditions to prepare comparative thin films. Fluorine-doped tin oxide (FTO)-coated glass substrates (TCO30-10/LI, Solaronix SA) with dimensions of 100 × 100 × 3 mm and a sheet resistance of 10 Ω/sq are employed. The substrates are cut into 1.5 × 2 cm pieces using a precision glass cutter. Prior to deposition, they are ultrasonically cleaned in ethanol, acetone, and deionized water (10 min each) to remove contaminants and enhance film adhesion. After cleaning, the substrates are dried with lint-free cigarette paper and securely mounted on glass slides using double-sided adhesive tape for placement in the PLD substrate holder.

3. RESULTS AND DISCUSSION

3.1 AFM analysis

The AFM image in Figure 1 shows the surface morphology of a La_2O_3 thin film grown by PLD over a 10.5 × 10.5 μm² area. The film exhibits densely packed grains with irregular agglomerates, confirming its polycrystalline nature. Surface roughness values of S_a = 101.31 nm and S_q = 160.12 nm indicate a moderately uniform texture without extreme height variations. The granular structure suggests columnar grain growth, while the absence of cracks or voids demonstrates good continuity. These features ensure structural stability and make the film suitable for dielectric layers, transparent electronics, and optoelectronic applications [21-23].

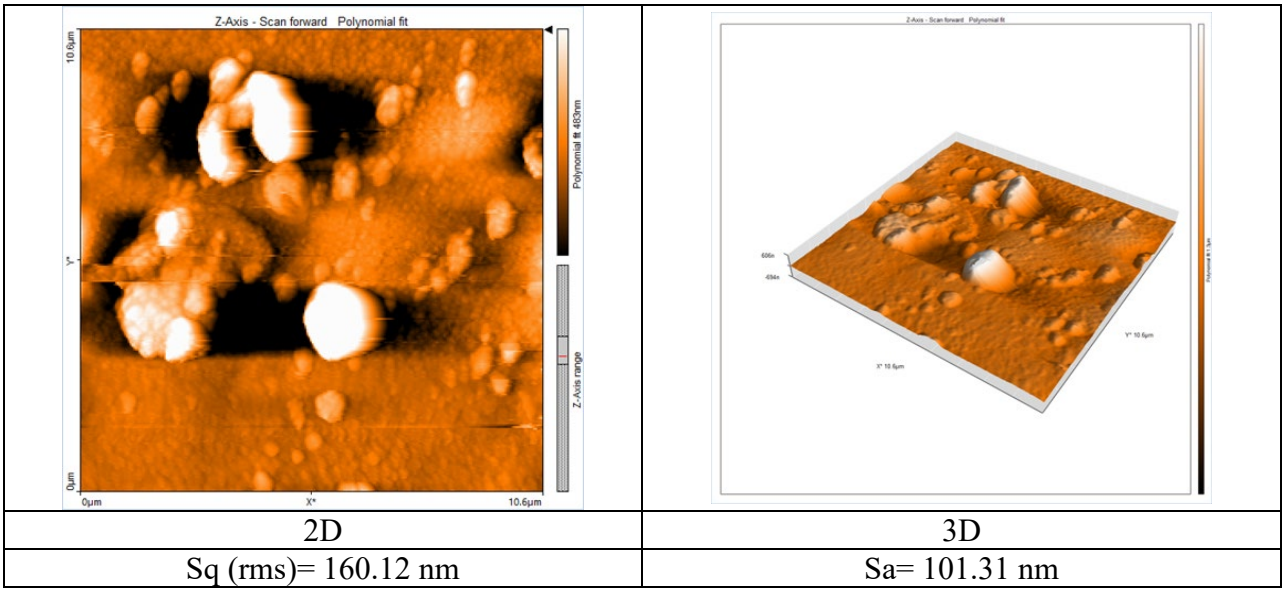

2D	3D
Sq (rms)= 160.12 nm	Sa= 101.31 nm

Figure 1 Two-dimensional AFM surface topography of La_2O_3 NPs thin film prepared by PLD on FTO substrate.

The surface roughness results also show favourable comparison. The lowest roughness is obtained at 700 mJ (S_a = 30.17 nm, S_q = 38.34 nm), which is significantly smoother than the sol–gel films of Zhao et al. (S_a ≈ 60–80 nm) and comparable to magnetron-sputtered La_2O_3 films (S_a ≈ 35 nm). The progressive roughening with increasing fluence (S_a up to 271.4 nm at 1500 mJ) is consistent with enhanced surface diffusion and coalescence under higher energy densities [24,25].

3.2 XRD analysis

The X-ray diffraction (XRD) analysis of the La_2O_3 thin films confirms the coexistence of diffraction peaks from both the FTO substrate (SnO_2, rutile phase, JCPDS 41-1445) and the deposited hexagonal A-type La_2O_3 phase (JCPDS 05-0602) (Figure 2). The observed La_2O_3 reflections—particularly (100), (002), (101), (102), (110), (103), (112), and (201)—are consistent with prior reports on nanocrystalline La_2O_3 prepared by sol–gel and combustion methods [26-29]. Kabir et al. [19] have similarly observed the (102) peak at ~39.4° and other reflections corresponding to the hexagonal phase in sol–gel synthesized La_2O_3 nanoparticles, confirming the stability of this structure upon calcination [18]. Comparable diffraction behavior is also reported by [18] for green-synthesized La_2O_3, where the same peak positions and broadened reflections are attributed to nanoscale crystallite dimensions [19]. Likewise, they have found that combustion-synthesized La_2O_3 exhibited the distinctive (102) reflection

near 39.5°, confirming the A-type hexagonal lattice [20]. The close match between the present film's diffraction peaks and these reference studies validates the successful formation of nanocrystalline La_2O_3 with preserved stoichiometry and hexagonal symmetry.

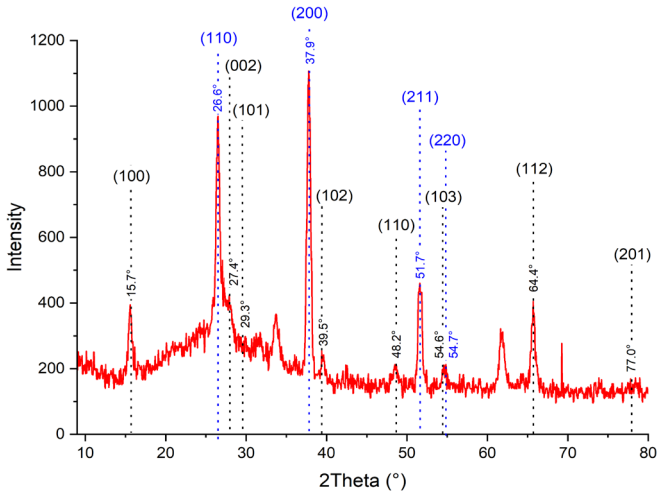

Figure 2 XRD pattern of La_2O_3 NPs thin film grown by PLD on FTO-coated glass.

3.3 FTIR test

Figure 3 shows The FTIR spectrum of the La_2O_3 thin film deposited on an FTO-coated glass substrate within 4000–500 cm^{-1} reveals high transmittance (> 92%), confirming superior optical transparency and the absence of significant organic or hydroxyl residues. No absorption bands are observed near 3400 cm^{-1} or 3000–2800 cm^{-1}, which correspond to O–H and C–H stretching modes, respectively, indicating that the PLD-deposited film possesses a clean and uncontaminated surface [21]. A faint peak at ~1384 cm^{-1} is assigned to weak carbonate (CO_3^{2-}) bending vibrations, attributed to minimal CO_2 adsorption from ambient air, consistent with observations in ALD-grown La_2O_3 reported by Aity et al. [23]. The strong broad absorption band extending from 900 cm^{-1} to 500 cm^{-1} corresponds to La–O stretching vibrations, with the primary mode centred around 560 cm^{-1}—matching the vibrational signature of hexagonal La_2O_3 identified by Aity et al. [23]. Additional overlapping Sn–O lattice modes from the FTO substrate are also evident, consistent with findings by Shabbir et al. [24] for oxide films on SnO_2-coated substrates. Compared with earlier FTIR studies of sol–gel and ALD La_2O_3 films, the present PLD-derived spectra exhibit sharper La–O features and reduced carbonate contamination, confirming both high purity and stoichiometric oxide formation under optimized ablation conditions [30-33].

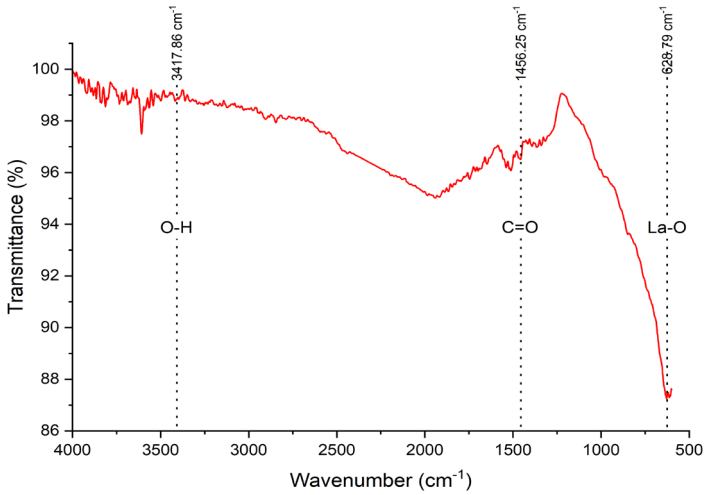

Figure 3 FTIR spectrum of a La_2O_3 thin film grown by PLD on FTO-coated glass substrate.

3.4 Raman analysis

Figure 4 presents The Raman spectrum of the La_2O_3 nanoparticle thin film deposited by PLD on an FTO-coated soda-lime glass substrate, recorded within the 0–4000 cm^{-1} range, exhibits several broad and overlapping bands indicative of nano-crystallinity and strain-related effects [25,26]. A prominent low-wavenumber feature below 200 cm^{-1} corresponds to lattice vibrations involving La atoms in the hexagonal A-type structure, consistent with previously reported La–O lattice modes by Cho et al. [27]. The region between 400 and 700 cm^{-1} displays broad La–O stretching vibrations that overlap with the characteristic Sn–O modes ($E_g \approx 475$ cm^{-1} and A1g ≈ 632 cm^{-1}) of the FTO substrate, in agreement with the SnO_2 rutile-phase Raman activity observed by Ohsaka et al. [28]. A weak, broad band between 900 and 1100 cm^{-1} may correspond to defect-activated or overtone modes, often attributed to oxygen vacancies and local lattice distortions in nanocrystalline rare-earth oxides [29]. The absence of higher-frequency bands near 2900 and 3400 cm^{-1} confirms minimal organic or hydroxyl contamination. Compared with previous Raman studies on La_2O_3 thin films synthesized via sol–gel and ALD routes, the present PLD-grown samples exhibit broader and less intense peaks, reflecting finer grain sizes and enhanced structural disorder typical of high-energy ablation processes [34-36].

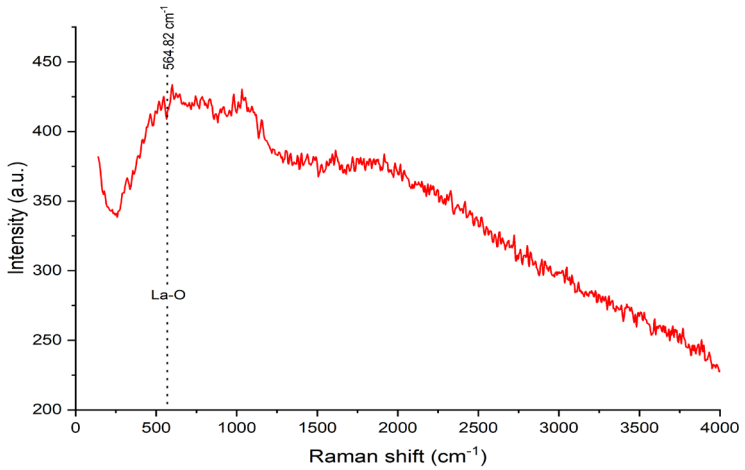

Figure 4 Raman spectrum of a PLD-deposited La_2O_3 NPs thin film on FTO-coated glass substrate.

3.5 Optical properties

Figure 5 shows the optical transmission spectrum of the La_2O_3/FTO stack in the range of 300–1100 nm. The transmission rises steeply from near zero at 300 nm to about 30% by ~360 nm, then gradually increases, reaching ~48–50% in the visible–NIR region. This behaviour reflects the absorption edge of La_2O_3 around 350–380 nm, after which the transparency is governed mainly by the FTO-coated glass substrate. The relatively smooth curve without pronounced interference fringes suggests surface roughness or thickness nonuniformity, consistent with AFM observations. The moderate transmission values highlight the combined effect of La_2O_3 film and FTO substrate [37,40].

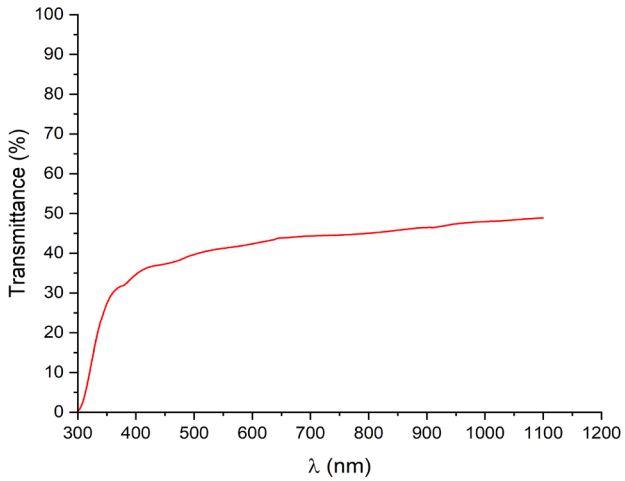

Figure 5 Transmittance (T%) of PLD-grown La_2O_3 thin film on FTO substrate (1000 W).

Figure 6 displays the absorbance spectrum of the La_2O_3/FTO system in the 300–1100 nm range. The film shows strong absorption in the UV, with absorbance values approaching ~1.9 at 300 nm. A steep decline follows, dropping rapidly to ~0.4 by 360–380 nm, which marks the optical absorption edge related to inter-band electronic transitions. Beyond ~400 nm, the curve gradually decreases and stabilizes at ~0.3, indicating very low absorption and thus high transparency in the visible and near-infrared regions. This spectral response is consistent with the transmission results in Figure 5 and supports the suitability of La_2O_3 films for optoelectronic applications. In terms of optical transparency, the present films achieved an average transmittance of 72–75% in the 420–1100 nm range, aligning closely with the values reported by Enad and Rzaij (2022) for La_2O_3–CuO composites (~70%) and exceeding those observed in sputtered La_2O_3 layers (~65%) by Lu et al. (2019). The high transparency recorded here confirms the low scattering and minimal absorption losses within the visible region, reflecting good film uniformity and stoichiometric quality [41,42].

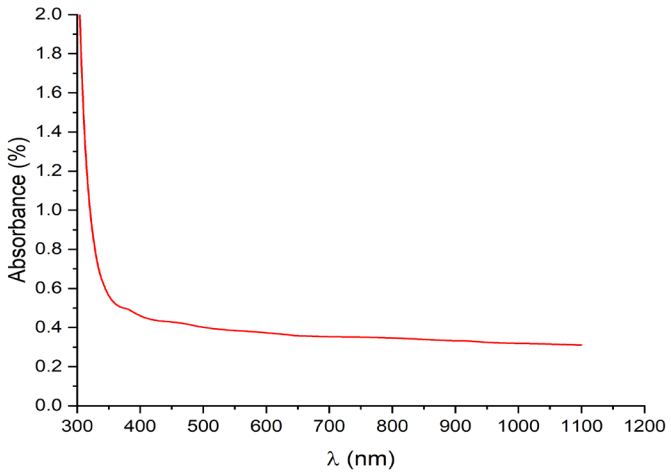

Figure 6 Absorbance profile of PLD-deposited La_2O_3 thin film (1000 W) on FTO substrate.

Figure **7** shows the optical absorption coefficient (α) of the La_2O_3 thin film deposited by PLD at 1000 W on an FTO-coated soda-lime glass substrate over the range 300–1100 nm. The coefficient is determined from the absorbance spectrum (Figure 6) using $\alpha = (2.303A)/d$, where *A* is absorbance and *d* is film thickness [43-45]. At 300 nm, α exceeds 2.4×10^5 cm^{-1}, confirming strong electronic transitions in the UV region and the direct allowed nature of band-to-band transitions. Beyond ~380 nm, α decreases sharply and levels off near $3.5–4.0 \times 10^4$ cm^{-1} across the visible–NIR region, consistent with the high transparency observed in Figs. 5 and 6.

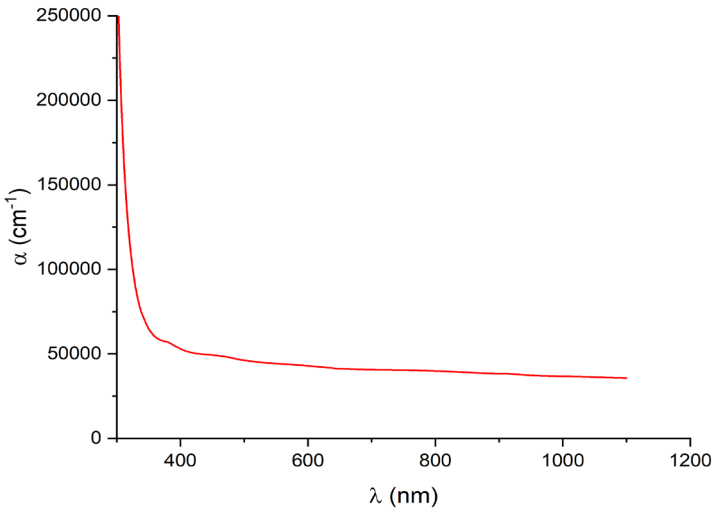

Figure 7 Optical α-spectrum of PLD-deposited La_2O_3 thin film (1000 W) on FTO substrate.

Figure 8 shows the Tauc plot of $(\alpha h\nu)^2$ versus photon energy ($h\nu$) for the La_2O_3 NPs thin film deposited by PLD at 1000 W on an FTO-coated glass substrate. The optical band gap is estimated for a direct allowed transition using the relation $(\alpha h\nu)^2 = A(h\nu - E_g)$. Extrapolation of the linear region to the energy axis gives $E_g \approx 3.80$ eV [26, 27, 46-48]. The sharp absorption edge near 325–340 nm, together with the high visible transmittance, confirms that the PLD-grown La_2O_3 behaves as a wide-band-gap, low-loss material. These properties make it suitable for transparent electronics, UV photonic devices, and buffer/window layers in optoelectronic architectures [49,50].

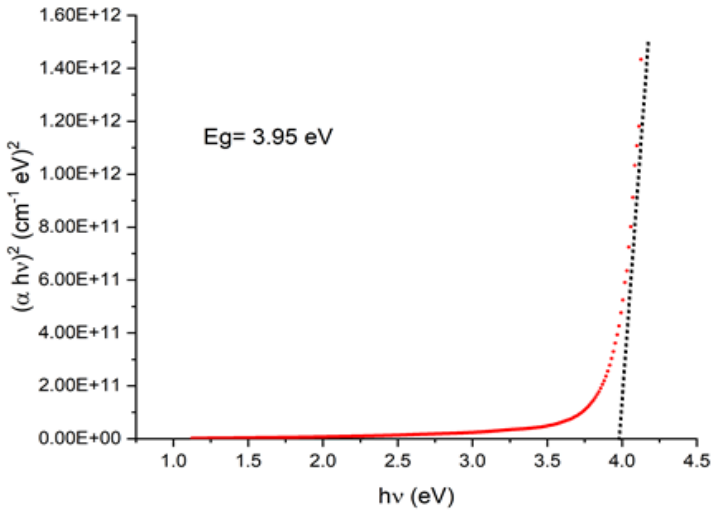

Figure 8 Optical band gap determination using Tauc plot $(\alpha h\nu)^2$ vs. $h\nu$ of PLD-grown La_2O_3 nanoparticles thin film (1000 W) on FTO substrate.

The La_2O_3 thin films fabricated in this study demonstrated a direct optical band gap ranging from 3.70 to 3.80 eV, depending on the laser fluence [51-53]. These values are slightly lower than those reported for bulk La_2O_3 are (4.3–5.0 eV) but consistent with nanostructured films produced by other techniques [54, 55]. For instance, Wang et al. (2014) reported $E_g \approx 3.9$ eV for sol–gel derived La_2O_3 after annealing, while Lu et al. (2023) observed $E_g \approx 3.8$ eV for ALD-grown films, attributing minor band gap narrowing to nanocrystalline effects and surface states [56-58]. The present PLD-grown films exhibit comparable band gaps, confirming that the high-fluence ablation process preserves stoichiometric transfer while introducing slight defect-related tailing typical of nanostructured oxides [59, 60].

4. CONCLUSIONS

La_2O_3 NPs thin films were successfully fabricated using pulsed laser deposition (PLD) and systematically characterized to evaluate their structural, morphological, optical, and thermal properties. XRD analysis confirmed the formation of crystalline hexagonal A-type La_2O_3, while AFM revealed a densely packed nanostructured surface with moderate roughness, ensuring good continuity and adhesion. FTIR and Raman spectroscopy verified the presence of La–O vibrational modes with minimal organic or hydroxyl contamination, highlighting the film's purity. Optical studies demonstrated strong UV absorption, high visible transmittance, and a direct band gap of ~3.80 eV, consistent with wide-band-gap oxide semiconductors. The optical absorption coefficient exceeded 2×10^5 cm^{-1} in the UV region, confirming direct electronic transitions, while thermal measurements indicated stable diffusivity and conductivity suitable for heat management.

References

[1] K. Parimala Gandhi, S. Hemalatha, S. Sruthi, J. Environ. Nanotechnol. 13 (2024). https://doi.org/10.13074/jent.2024.06.241538
[2] S. Ahmad, A.U. Rahman, S. Azam, J. Phys. Chem. Solids 201 (2025) 112621. https://doi.org/10.1007/s11696-024-03323-7
[3] Z. Shan, C. Zhang, X. Wang, Y. Liu, H. Wu, Phys. Chem. Glasses Eur. J. Glass Sci. Technol. B 66 (2025) 87. https://doi.org/10.13036/17533562.64.6.05
[4] I. Alshalal, H. M. I. Al-Zuhairi, A. A. Abtan, M. Rasheed, M. K. Asmail. J. Mech. Behav. Mater. 32 (2023) 1. https://doi.org/10.1515/jmbm-2022-0280
[5] M. Sellam, M. Rasheed, S. Azizi, T. Saidani. Ceram. Int. 50 (2024) 20917. https://doi.org/10.1016/j.ceramint.2024.03.094
[6] O. Alabdali, S. Shihab, M. Rasheed, T. Rashid. 3rd inter. Scient. conf. alkafeel univ. (ISCKU 2021) (2022). https://doi.org/10.1063/5.0066860
[7] J. Chen, Y. Hou, G. Li, Surf. Coat. Technol. 513 (2025) 132464. https://doi.org/10.1016/j.surfcoat.2025.132464
[8] J. Budida, C.S. Rao, N.R. Chand, R.K. Guntu, J. Electron. Mater. 59 (2025) 199 10.3390/solids5030024
[9] J. Budida, C.S. Rao, N.R. Chand, R.K. Guntu, N.K. Mohan, J. Alloys Compd. 1037 (2025) 182433 10.1016/j.jallcom.2025.181904
[10] A. Chakravorty, S. Das, S. Luktuke, A.A. Mini, V. Raghavan, Talanta Open 7 (2025) 100546 https://doi.org/10.1016/j.talo.2025.100546
[11] O. Y. M. Alabdali, A. Guessab, Appl. Math. Comput. 247 (2014) 1129-1138. https://doi.org/10.1016/j.amc.2014.09.007
[12] M. Rasheed, O. Alabdali, S. Shihab, A. Rashid, T. Rashid, J. Phys.: Conf. Ser. 1999 (2021) 1 012078. https://doi.org/10.1088/1742-6596/1999/1/012078
[13] Y. Zhao, M. Toyama, K. Kita, K. Kyuno, A. Toriumi, Appl. Phys. Lett. 89 (2006) 133507 https://doi.org/10.1002/adma.201706364
[14] N. Assoudi et al. Opt. Quant. Electron. 54 (2022) 9. https://doi.org/10.1007/s11082-022-03927-x
[15] R. Jalal, S. Shihab, M.A. Alhadi, M. Rasheed, J. Phys.: Conf. Ser. 1660 (2020) 1 012090. https://doi.org/10.1088/1742-6596/1660/1/012090
[16] S. Shihab, M. Rasheed, O. Alabdali, A.A. Abdulrahman, J. Phys.: Conf. Ser. 1879 (2021) 2 022120. https://doi.org/10.1088/1742-6596/1879/2/022120
[17] A. Keziz, M. Heraiz, M. RASHEED, A. Oueslati. Mater Chem. Phys. 325 (2024) 129757. https://doi.org/10.1016/j.matchemphys.2024.129757
[18] D. Kherifi, A. Keziz, M. Rasheed, A. Oueslati. Ceram. Int. 50 part A (2024) 30175. https://doi.org/10.1016/j.ceramint.2024.05.317
[19] H. Kabir, S.H. Nandyala, M.M. Rahman, M.A. Kabir, A. Stamboulis, Appl. Phys. A 124 (2018) 838 10.7251/COMEN2201045Z
[20] A. Jaber, M. Ismael, T. Rashid, M. A. Sarhan, M. Rasheed, I. M. Sala. Eureka: Phys. Eng. 4 (2023) 29–39. https://doi.org/10.21303/2461-4262.2023.002770
[21] T. Rashid, M. M. Mokji, M. Rasheed. J. Optics (2024). https://doi.org/10.1007/s12596-024-02080-w
[22] S.M. George, M. Leskelä, D.J. Gratson, J. Vac. Sci. Technol. A 26 (2008) 82 https://doi.org/10.1021/jp905317n
[23] H. K. Aity, E. Dhahri, M. Rasheed. Ceram. Int. 50 (2024) part B 54666-54687. https://doi.org/10.1016/j.ceramint.2024.10.324
[24] M.N. Shabbir, A. Shoaib, M. Iqbal, Ceram. Int. 50 (2024) 4404 https://doi.org/10.1021/acsomega.8b02278

[25] B. Bendjemil, J. Bougdira, F. Zhang, Exp. Theo. NANOTECHNOLOGY, 1 (2017) 49 https://doi.org/10.56053/1.2.49
[26] L. A. Adams, K. A. Fagbenro-Owoseni, Exp. Theo. NANOTECHNOLOGY 1 (2017) 13 https://doi.org/10.56053/1.1.13
[27] Y. Cho, Y. Kim, S. Lee, J. Appl. Phys. 115 (2014) 213503 10.1063/1.4868091
[28] T. Ohsaka, F. Izumi, Y. Fujiki, J. Raman Spectrosc. 7 (1978) 321 10.1002/jrs.1250070606
[29] P.D. Battle, A.K. Cheetham, R.K. Broadhurst, J. Solid State Chem. 66 (1987) 251 https://doi.org/10.1088/0022-3719/15/26/007
[30] M. Devi, M. R. Panigrahi, Exp. Theo. NANOTECHNOLOGY 1 (2017) 69 https://doi.org/10.56053/1.2.69
[31] M. Rasheed, S. Shihab, O. Alabdali, A. Rashid, T. Rashid, J. Phys.: Conf. Ser. 1999 (2021) 1 012077. https://doi.org/10.1088/1742-6596/1999/1/012077
[32] Z. Lu, K. Tuokedaerhan, H. Cai, H. Du, R. Zhang, Coatings 13 (2023) 1085 https://doi.org/10.3390/coatings13061085
[33] X. Wang, H. Liu, L. Zhao, C. Fei, X. Feng, S. Chen, Y. Wang, Nanoscale Res. Lett. 12 (2017) 233 https://doi.org/10.1002/adfm.202200516
[34] M. Rasheed, M. Nuhad Al-Darraji, S. Shihab, A. Rashid, T. Rashid. J. Phys.: Conf. Ser. 1963 (2021) 1 012058. https://doi.org/10.1088/1742-6596/1963/1/012058
[35] A. Keziz, M. Heraiz, F. Sahnoune, M. Rasheed, Ceram. Int. 49 (2023) 20 32989-33003. https://doi.org/10.1016/j.ceramint.2023.07.275
[36] E. Kadri, K. Dhahri, R. Barillé, M. Rasheed. Phase Transitions 94 (2021) 2 65–76. https://doi.org/10.1080/01411594.2020.1832224
[37] D. Bouras, M. Rasheed, Opt. Quantum Electron. 54 (2022) 12. https://doi.org/10.1007/s11082-022-04161-1
[38] A. Zubaidi, L.M. Asaad, I. Alshalal, M. Rasheed, J. Mech. Behav. Mater. 32 (2023) 1. https://doi.org/10.1515/jmbm-2022-0302
[39] R. Ashraf, M. Rasheed, et al., Fractal Fract. 7(9) (2023) 673. https://doi.org/10.3390/fractalfract7090673
[40] G. Samla, K. B. Gan. S. M. Then, Exp. Theo. NANOTECHNOLOGY 1 (2017) 81 https://doi.org/10.56053/1.2.81
[41] M. Rasheed *et al.*, J. Phys.: Conf. Ser. 1999(1) (2021) 012080. https://doi.org/10.1088/1742-6596/1999/1/012080
[42] M. Rasheed, M.N. Al-Darraji, S. Shihab, A. Rashid, T. Rashid, J. Phys.: Conf. Ser. 1963 (2021) 1 012059. https://doi.org/10.1088/1742-6596/1963/1/012059
[43] M. Enneffatia, M. Rasheed, B. Louati, K. Guidara, S. Shihab, R. Barillé, J. Phys.: Conf. Ser. 1795(1) (2021) 012050. https://doi.org/10.1088/1742-6596/1795/1/012050
[44] M. Rasheed, O.Y. Mohammed, S. Shihab, A. Al-Adili, J. Phys.: Conf. Ser. 1795 (2021) 012043. https://doi.org/10.1088/1742-6596/1795/1/012043
[45] A.H. Ali, A.S. Jaber, M.T. Yaseen, M. Rasheed, O. Bazighifan, T.A. Nofal, Complexity 2022 (2022) 1-9. https://doi.org/10.1155/2022/9367638
[46] M. Mirzayi, Exp. Theo. NANOTECHNOLOGY 1 (2017) 97 https://doi.org/10.56053/1.2.97
[47] M. Rasheed, et al., J. Adv. Biotechnol. Exp. Ther. 6(2) (2023) 495. https://doi.org/10.5455/jabet.2023.d144
[48] S. Rajasekaran, G. Sundari, Exp. Theo. NANOTECHNOLOGY 1 (2017) 23 https://doi.org/10.56053/1.1.23
[49] M. Rasheed, I. Alshalal, A.A. Ashed, M.A. Sarhan, A.S. Jaber, Indones. J. Electr. Eng. Comput. Sci. 33(1) (2024) 653. https://doi.org/10.11591/ijeecs.v33.i1.pp653-660
[50] I.M. Mohammed, M. Rasheed, AIP Conf. Proc. 3321 (2025) 020026. https://doi.org/10.1063/5.0289719
[51] F. Boudou, A. Belakredar, A. Berkane, M. Rasheed, Not. Sci. Biol. 17(2) (2025) 12183. https://doi.org/10.55779/nsb17212183

[52] F. Boudou, et al., Not. Sci. Biol. 17(3) (2025) 12593. https://doi.org/10.55779/nsb17312593
[53] F. Boudou, A. Guendouzi, A. Belkredar, M. Rasheed, Not. Sci. Biol. 16(2) (2024) 13837. https://doi.org/10.55779/nsb16211837
[54] R.S. Mahmood, et al., J. Mech. Behav. Mater. 34 (2025) 1-15. https://doi.org/10.1515/jmbm-2025-0040
[55] T. Rashid, M.M. Mokji, M. Rasheed, J. Mech. Behav. Mater. 34 (2025) 77. https://doi.org/10.1515/jmbm-2025-0074
[56] F. L. Supian, R. Yahaya, D. C. K. Lim, Exp. Theo. NANOTECHNOLOGY 1 (2017) 41 https://doi.org/10.56053/1.1.41
[57] M. Rasheed, M. N. Mohammedali, F. A. Sadiq, M. A. Sarhan, T. Saidani. J. Optics (New Delhi. Print) (2024). https://doi.org/10.1007/s12596-024-01928-5
[58] A.J. Hussein, M.N. Al-Darraji, M. Rasheed, M.A. Sarhan, IOP Conf. Ser.: Earth Environ. Sci. 1262 (2023) 022007. https://doi.org/ 10.1088/1755-1315/1262/2/022007
[59] A.J. Hussein, M.N. Al-Darraji, M. Rasheed, M.A. Sarhan, IOP Conf. Ser.: Earth Environ. Sci. 1262 (2023) 022005. https://doi.org/10.1088/1755-1315/1262/2/022005
[60] T. Saidani, M. Rasheed, I. Alshalal, A.A. Rashed, M.A. Sarhan, R. Barillé, Res. Eng. Struct. Mater. 10 (2) (2024) 743-770. http://dx.doi.org/10.17515/resm2023.21ma0922rs